
# A simplified aortic ring assay: A useful *ex vivo* method to assess biochemical and functional parameters of angiogenesis

**Aastha Kapoor, Carolyn G. Chen and Renato V. Iozzo**

***Department of Pathology,*** *Anatomy and Cell Biology and the Cancer Cell Biology and Signaling Program, Kimmel Cancer Center, Sidney Kimmel Medical College at Thomas Jefferson University, Philadelphia, PA, USA*

***Correspondence to Renato V. Iozzo:*** *renato.iozzo@jefferson.edu*
https://doi.org/10.1016/j.mbplus.2020.100025

## Abstract

We present a simplified method for conducting aortic ring assays which yields robust sprouting and high reproducibility targeted towards matrix biologists studying angiogenesis and extracellular matrix signaling. Main adjustments from previously established protocols include embedding aortic rings between two layers of 3D type I collagen matrix and supplementing with vascular endothelial media. We also introduce a concise and effective staining protocol for obtaining high-resolution images of intracellular and extracellular matrix proteins along with a more accurate protocol to quantify angiogenesis. Importantly, we present a novel method to perform biochemical analyses of vessel sprouting without contamination from the aortic ring itself. Overall, our refined method enables detection of low abundance and phosphorylated proteins and provides a straightforward *ex vivo* angiogenic assay that can be easily reproduced by those in the matrix biology field.


## Introduction

Angiogenesis, the formation of new blood vessels from existing vasculature, is a physiological and necessary process of growth and wound healing that encompasses the dynamic paracrine signaling between various cell types [1], growth and pro-angiogenic factors [2,3], cytokines, and neuronal influences [4]. The powerful interplay between the burgeoning vasculature and the surrounding extracellular matrix molecules is critical to this process [5–13] and is of increasing interest to those studying the matrix in the context of wound healing, cancer and inflammation [14–19].

Over the past twenty years, *ex vivo* models of angiogenesis, such as vascular explant cultures, have gained increasing prominence as they overcome the limitations posed by *in vitro* techniques and simplify the complexity presented in *in vivo* models. As an investigative link between *in vitro* and *in vivo* angiogenic assays, the aortic ring assay is the most widely-performed *ex vivo* model for studying angiogenesis to date. This method provides a large sample size, high reproducibility and low cost. First pioneered by Nicosia et al. in 1982 using rat aorta [20], the protocol has been since modified for a whole host of species including: mouse, chicken, rabbit, cow, dog, and human. This assay has also progressed beyond the aorta to other large vessels such as the carotid artery, vena cava, thoracic duct, and saphenous vein [21–25]. More recently, *ex vivo* angiogenic assays have extended to include explants from highly-vascularized regions such as the choroid and epididymis [26,27].

In the present study, we report a simplified and refined protocol for performing aortic ring assay on mouse aorta, distilling each component of the assay and methods of analyses into concise and reproducible steps for those studying angiogenesis with a focus on extracellular matrix. Importantly, we introduce a streamlined method for visualizing and quantifying intra- and extracellular proteins in neovessels migrating from the aortic ring and offer a concise protocol for performing biochemical and immunological analyses exclusively on vessel sprouts.

## Results and discussion

### A simplified aortic ring assay (Fig. 1)

The aortic ring assay is biologically superior in recreating steps of angiogenesis compared to *in vitro* assays. It encompasses initial vessel sprouting, followed by matrix remodeling and lumenization of the vessels. Besides, aortic ring sprouts anatomically mimic *in vivo* microvessels making it suitable for paracrine signaling studies among endothelial cells, pericytes and the smooth muscle cells. Any genetic manipulations and physical treatments given to the mouse are translatable to the aorta and the effect is measurable as difference in ring sprouting.

Here, we report a simplified aortic ring assay that is useful to investigators involved in matrix biology, angiogenesis and extracellular matrix signaling. This concise method encompasses the three steps in Fig. 1. We provide an overview of each step summarized in Fig. 1 with additional notes presented in the Experimental Procedures.

Step 1. Preparation of 3D collagen type I matrix

A. *Collagen preparation*: For one mouse aorta, prepare 3.155 ml collagen matrix for 20 wells (total 150 µl/well). Under a sterile laminar flow hood, first mix 135 µl filtered and autoclaved water, 1.25 ml 140 mM $NaHCO_3$, 10 µl 1 M NaOH, and 460 µl 10 × 199 Media to an ice-

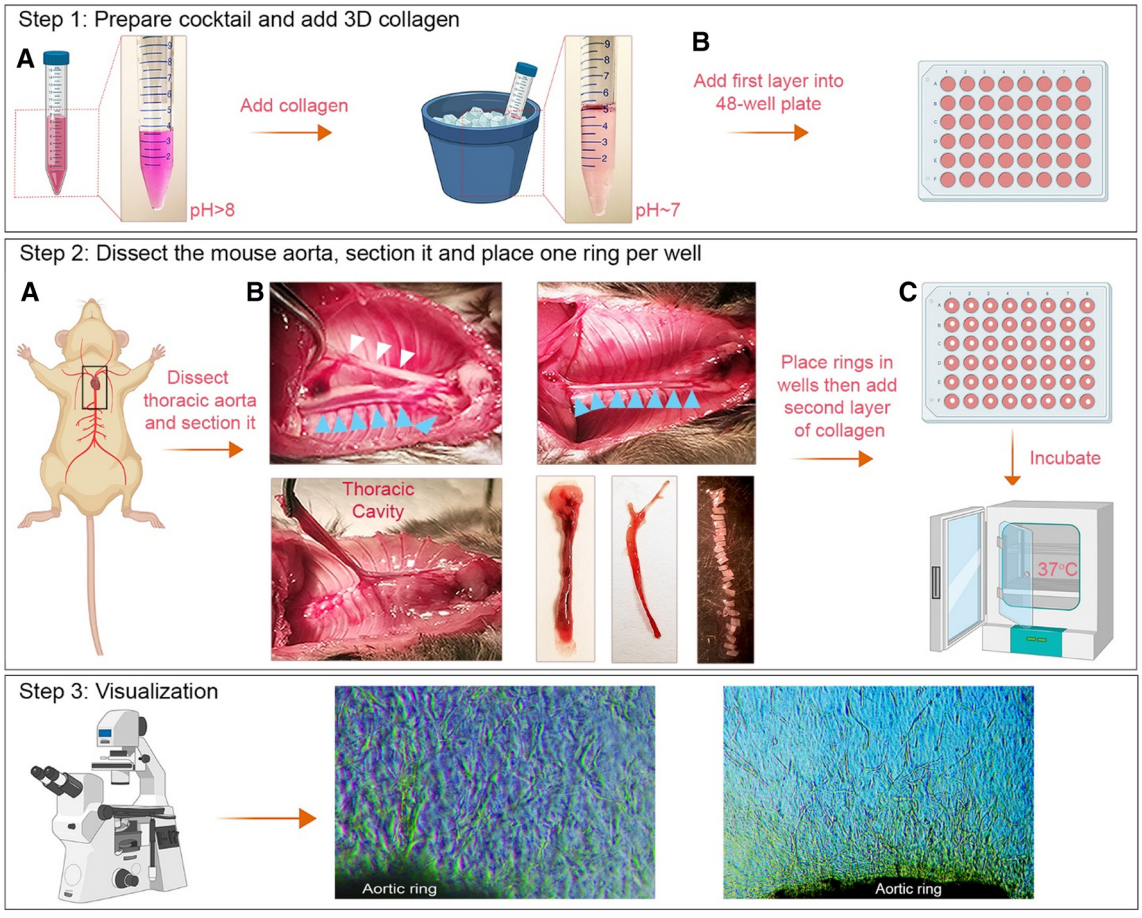


**Fig. 1.** Aortic ring dissection protocol. Step 1 (A) To make the 3D collagen type I solution, add water, $NaHCO_3$, NaOH, and 10 × 199 Media to a pre-chilled 15 ml tube on ice. Add pre-chilled rat-tail type I collagen, mix thoroughly on ice by pipetting, and adjust pH to 7.0 using 1 M NaOH. (B) Pipette 100 µl/well of collagen in 48-well plate and incubate at 37 °C for 30 min. Step 2 (A) Euthanize mouse and dissect out the thoracic aorta by exposing the chest cavity and removing heart, lungs, and esophagus. Remove esophagus (blue arrows) from aorta (white arrows) and use forceps and scalpel to detach aorta from the spine. After removing surrounding tissue and fat, section aorta into approximately 20 rings of ~1 mm width. (B) Gently place one ring/well in polymerized 3D collagen type I matrix, add 50 µl pre-chilled collagen as a second layer and incubate at 37 °C for 30 min. Add 100 µl endothelial media to each well and incubate. Step 3 (A) To visualize ring sprouting, use a light microscope with the phase-contrast setting. (B) Phase contrast images of sprouted rings on day 8–12 with magnification from 5× to 60×. Images were pseudo-colored in Photoshop for enhanced contrast.

cold tube and mix thoroughly by pipetting[1]. Next, add 1.3 ml of rat-tail type I collagen (3 mg/ml in 20 mM $CH_3COOH$) for a final volume of 3.155 ml and mix thoroughly by pipetting. Adjust the pH to 7 using 1–2 drops of 1 M NaOH[2].

B. *First collagen layer*: Place 100 µl/well of collagen in 48-well plate and incubate at 37 °C for 30 min to facilitate collagen polymerization[3]. Keep the remaining collagen preparation on ice for the second layer.

Step 2. Dissection of C57BL/6 J mice aorta

A. *Aortic dissection*: Following euthanasia, expose the thoracic cavity of the mouse and remove heart, lungs, and esophagus (white arrows)[4]. Remove the thoracic aorta (blue arrows) from the spine with clean forceps and scalpel. Wash aorta in Hank's Balanced Salt Solution (HBSS) and transfer to a hard dissection surface under a stereoscopic microscope. Remove excessive fat surrounding the aorta with a sharp blade and section aorta into 20 rings of ~1 mm width.
B. *Aortic ring placement on 3D collagen*: Using forceps, gently place one ring/well onto the polymerized collagen layer. Under the hood, add the second layer of collagen (50 µl) to fully cover the aortic rings and incubate for 30 min at 37 °C. Add 100 µl of endothelial media[5] to each well. Replace media every 3 days.

Step 3. Visualization of rings

A. *Phase contrast imaging of sprouted rings*: To monitor proper sprouting in real time, place the explants under a light microscope using phase-contrast and equipped with a digital camera. We typically observed sprouting by day 3 with maximal sprouting observed at day 9.
B. *Visualization of rings*: Visualize ring sprouting with magnification ranging from 5× to 60×. Images may be pseudo-colored using the *hue/saturation* setting in Photoshop for enhanced contrast.

## A simplified quantification method of sprouting area (Fig. 2)

*Radial distance of the sprouts*: First, acquire the phase contrast images of live explants (Fig. 2A). Then, using the *subtract background* function in ImageJ (https://imagej.net/Fiji/Downloads), remove the background from each image using the rolling ball radius of 700 pixels (Fig. 2B). This step reduces noise and improves contrast. Next, using the *adjust threshold* function, exclusively highlight the sprouts, eliminating the aortic ring and any empty spaces (Fig. 2C). Finally, using the *set scale* function, input the accurate pixel/micron ratio based on the resolution settings of the microscope and magnification of the objective lens (*i.e.* 0.645 µm/pixel) and check the *global setting* option. Using the circle option on the ImageJ toolbar, draw a circle around the highlighted sprouts and another around the aortic ring. Use the *measure* function to determine the radii of each circle and subtract the radius of the larger circle from that of the smaller one to calculate the approximate radial distance of the sprouts (Fig. 2D).

## Confocal imaging and fluorescence quantification (Fig. 3)

A. *Aortic ring staining*: First, fix the rings in 100 µl of 4% paraformaldehyde (PFA) for 1 h on ice, wash them twice in 100 µl PBS[6] and permeabilize them with 250 µl 0.1% TritonX-100 for 20 min for staining intracellular proteins only[7]. Block the rings with 1% BSA/PBS for 2 h on the rocker at RT, and add the appropriate primary antibody[8] for 3 h. Wash with PBS three times, 15 min each, add secondary antibodies (1:400) for 1 h, stain the nuclei

[1] Keep collagen preparation on ice always to prevent polymerization. Pre-chill all reagents, pipette tips, and falcon tubes to 4 °C before use.
[2] We recommend using pH strips instead of a pH meter due to the viscosity and low volume. Note that the color of the collagen preparation changes based on the pH (basic is dark pink, acidic is yellow). The final color of the collagen preparation should change from dark pink to light pink after neutralization.
[3] Aortic rings are embedded between two layers of 3D collagen, 100 µl in the first layer and 50 µl in the second layer.
[4] Do not confuse the esophagus for the aorta, as the esophagus lies right above the aorta.
[5] For culturing the aortic rings, we compared two endothelial cell specific media, Lonza EGM-2 MV media (endothelial growth media-2 microvascular media) and VascuLife EnGS endothelial cell media. As DMEM is inefficient in promoting sprouting [39], we chose endothelial specific media. The major ingredients of both media are listed in Table 1. EGM-2 media is serum enriched (5% FBS) with VEFG present as one of the growth supplements, on the other hand EnGS media is a low-serum (2% FBS) media without any VEGF supplementation. Being richly supplemented EGM-2 media gave two times more growth than EnGS. Use of EGM-2 should be restricted to studies that do not involve VEGF or FGF while EnGS can be used for all studies.
[6] Rings can be stored in PBS after washing off PFA for a week before using for staining.
[7] Avoid this step when staining for HABP as detergent can disrupt HA deposition.
[8] Dilutions for IF staining: CD31 (1:200), P-PERK (1:200), HAS2 (1:200), IB4 (1:400).

**Table 1.** Composition of two endothelial cell culture media with low and high serum concentration.

| Component | Role of each component | Amount | |
|---|---|---|---|
| | | EnGS | EGM-2 |
| FBS (fetal bovine serum) | Contains growth factors, hormones, binding proteins, fatty acids and lipids and facilitates osmotic regulation | Low serum 10 ml (2%) | High serum 25 ml (5%) |
| VEGF (vascular endothelial growth factor) | Binds VEGFRs and promotes angiogenesis | Absent | 500 µl |
| FGF (fibroblast-derived growth factor) | Promotes overall endothelial cell growth. | Absent | 2 ml |
| Ascorbic acid | Increases the deposition of basement membrane related protein collagen IV | 500 µl | 500 µl |
| Hydrocortisone | Increases endothelial cell proliferation | 200 µl | 500 µl |
| Glutamine | Supplies TCA cycle with glutamate and α-ketoglutarate | 25 ml | Absent |
| EGF (epidermal growth factor) | Stimulates growth | 500 µl | 500 µl |
| IGF1 (Insulin-like growth factor 1) | Facilitates tube formation during angiogenesis | Absent | 500 µl |
| Heparin | Facilitates binding of growth factors like FGF or EGF to their receptors | 500 µl | Absent |
| EnGS (endothelial growth supplement) | Proprietary composition; does not contain VEGF | Absent | 1 ml |

with DAPI (1:1000) for 10 min in the dark, wash with PBS three times and visualize in PBS[9].

B. *Visualization of sproutings using confocal imaging*: Visualize the rings using confocal microscopy by directly placing the 48-well plate on the stage[10]. We provide examples of confocal images labeled with endothelial markers such as IB4 and CD31 (Fig. 3A) and dually-labeled sprouts with IB4 and hyaluronan-binding protein (HABP) (Fig. 3B). Also, we can visualize intracellular proteins, such as phosphorylated ($Thr^{980}$) PERK, following permeabilization with Triton X-100 (Fig. 3C). Use confocal software to acquire z-stack images with slice distance of 20–30 µm and convert them into maximum intensity projection (MIP) images[11].

C. *Quantification of fluorescently-labeled sproutings*: Using the *polygon selection* tool in ImageJ, quantify the sprouting area using confocal images by outlining the sprouts—thereby eliminating the aortic ring—and measuring the mean fluorescence intensity of the covered areas in integrated pixel/µm$^2$ (Fig. 3D). To compare among different conditions, normalize each fluorescence intensity value (*i.e.* images taken at different time points or under diverse treatments) to the area with the maximal sprouting. This allows an accurate comparison of the fluorescence intensity from different conditions based on differential sprouting area[12].

[9] Visualize rings in PBS at 10×. For long-term storage, keep the rings immersed in sterile PBS at 4 °C. The rings can be stored for a few weeks, but you need to add more PBS and 0.01% $NaN_3$.

[10] The objective used for confocal microscopy should have a sufficient working distance to accommodate the plate.

[11] We use Zeiss ZEN Black software to process the z-stack images using the MIP function. Other comparable software, such as Imaris, may be used.

[12] To acquire images for quantification, use 10× magnification and position the ring consistently on one side of the quadrant.

### Extraction of vessel sprouts and immunodetection (Fig. 4)

*Acquisition of vessel sprout lysate*: To acquire cell lysates of vessel sprouting for biochemical analysis, gently remove endothelial media from the well with a pipette[13]. Next, add 50 µl of ice-cold RIPA buffer to each well, dislodge the rings and surrounding collagen matrix with a 1 ml pipette, and transfer all contents into a 1.5-ml microfuge tube. Pool three rings into a single microfuge tube, vortex vigorously for 5 min and remove the insoluble aortic rings with clean forceps. This avoids contamination from the ring and specifically extracts lysates from the sprouts. Finally, add 100 µl of 5× sample buffer[14], vortex and boil for 5 min. Soluble lysate volume should be 300 µl that can be subjected to classical Western immunoblotting and can load up to 7 lanes (40 µl/lane). Final lysate can also be subjected to immunoprecipitation and proteomics analysis. Quantification of protein bands may be performed using ImageJ. We provide qualitative examples of various immunoblottings (Fig. 4) using antibodies against structural proteins (myosin IIA, β-catenin, lamin A/C, α-tubulin, α-smooth muscle actin), transmembrane receptors (VEGFR2, EphA2, CD31), cytosolic enzymes (AMPK, GAPDH, PTEN), autophagic markers (p62, LAMP1, LC3) and secreted protein (VEGFA).

## Discussion

The extracellular matrix plays pivotal roles in several physiological and pathological conditions and contains cues for active cellular signaling

[13] Do not use vacuum suction to remove the media, as this will dislodge the entire 3D collagen gel.

[14] Our routine 5× sample buffer for 10 ml contains the following: 5 ml of glycerol, 2.5 ml Tris-HCl (1.25 M, pH 6.8), 0.4 ml of bromophenol blue (0.6%), and 1 g of SDS.

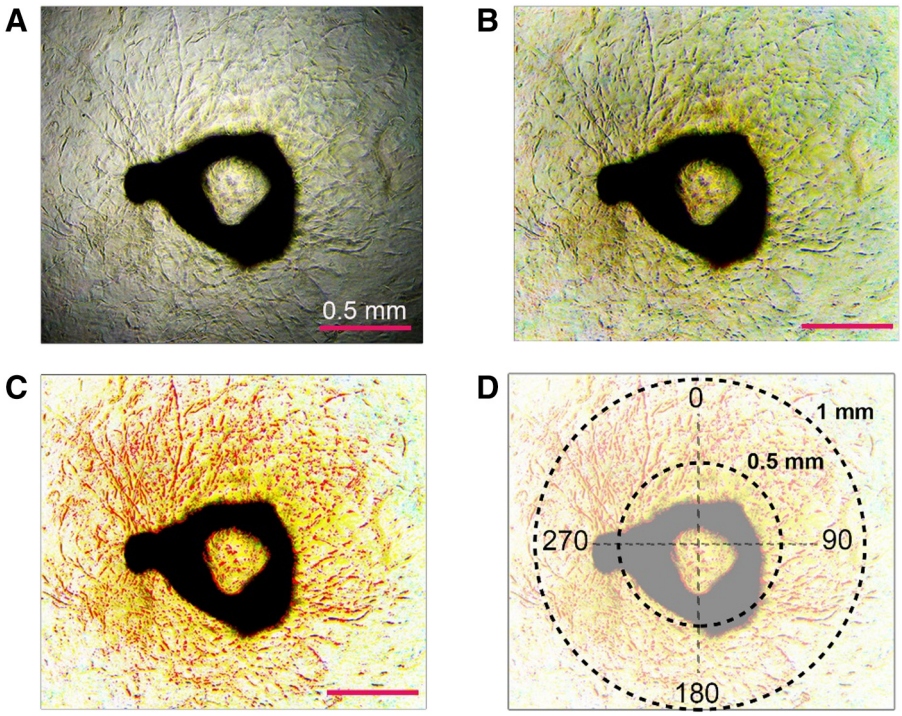


**Fig. 2.** Radial density quantification of ring sprouting. (A) Raw phase contrast image of sprouted ring after 8–10 days of incubation taken with 5× magnification. (B) Reduce background signal using *subtract background* function in ImageJ (rolling ball radius set to 700 pixels). (C) Highlight sprouts using the *adjust threshold* function in ImageJ. (D) Set the correct global pixel/micron ratio of the image (*i.e.* 0.645 μm/pixel) using the *set scale* function. Draw a circle around the sprouting edge and another around the aortic ring. Using the *measure* function, subtract the radius of the larger circle from the inner circle to calculate the approximate radial distance of angiogenesis.

mediated by canonical and non-canonical receptors involved in angiogenesis, wound healing, fibrosis and cancer [28–34]. It affects vascular fragility [35] and biomechanics of the tumor microenvironment [36]. One of the best *ex vivo* models to study angiogenesis and its molecular mechanism is the mouse aortic ring assay [22]. This model has been used to study interactions between endothelial and mural cells such as pericytes [37] and between endothelial cells and atherosclerosis plaque [38]. The rationale for this assay is based on the fact that, when embedded in a 3D collagen type I matrix, the endothelial cells lining the aortic intima are stimulated to migrate and form capillary-like structures that are fully lumenized. In our current method, we dissect the salient steps of this assay and present a simplified version for those interested in studying molecular angiogenesis. Beginning with a generalized overview of the assay in the results, we layout the protocol into three major steps and subsequently delve into the critical details. We provide high-resolution images of rare intracellular proteins such as P-PERK and HAS2 and showcase the distribution and organization of extracellular molecules, such as HA, surrounding the microvessels. We also discuss a more accurate and simplified method of protein quantification using phase contrast and fluorescence images. Finally, we provide a detailed protocol for solubilization of the sprouts and detection of several proteins by classical Western blotting including proteins involved in structural organization, growth, signaling and autophagy. Our improved protocol has broad implications. For example, extraction of proteins from ring lysates may be used for proteomic analysis, immunoprecipitation studies, and other biochemical methodologies.

Certain modifications in the aortic ring protocol accommodate prolific sprouting that is essential for obtaining high-quality images and reliable biochemical data. As pH widely affects viability of neo-endothelial cells, we first enhance the buffering capacity of the 3D collagen matrix by increasing the amount of sodium bicarbonate to 82 mM. In comparison, DMEM media, which has been routinely-used in collagen gels contains 42.8 mM sodium bicarbonate, which is insufficient to buffer the entire gel [22,39]. Second, we show that adding endothelial cell media—EGM-2 from Lonza or EnGS from Vasculife—to the collagen-embedded rings, significantly improved sprouting. Finally, we utilize a

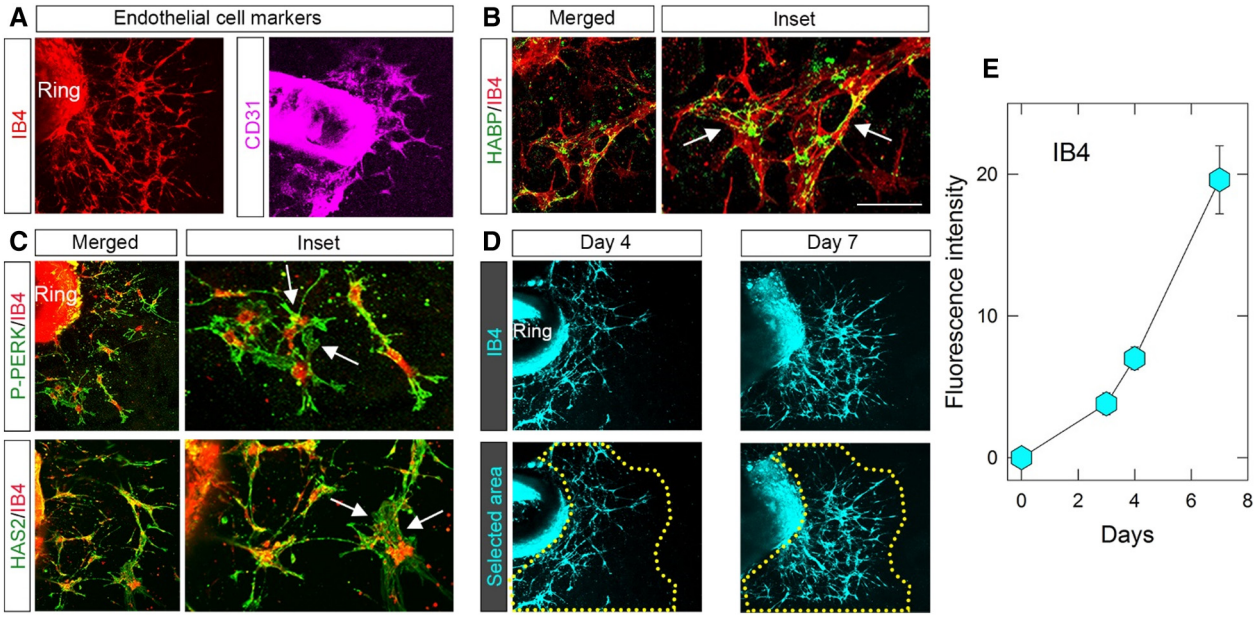


**Fig. 3.** Confocal imaging and fluorescence quantification of intra- and extra-cellular molecules. (A) Confocal images of aortic rings labeled with endothelial markers (IB4 and CD31) in red. Bar ~100 μm. (B) Images of aortic ring labeled with HABP (green) and IB4 (red). White arrows point to areas of HABP clearly identified outside the endothelium. (C) Images of aortic rings labeled for intracellular proteins P-PERK and HAS2 (green) and endothelial marker IB4 (red). Inset from the dotted rectangle (right), with white arrows pointing to intracellularly labeled proteins. (D) Aortic ring images labeled with IB4 (cyan). Yellow dotted line outlines the sprouting area. (E) Quantification of number of main sprouts and sprouting area of rings incubated from 0 to 7 days. Mean ± SEM. Ring marks the aortic ring.

collagen sandwich model, embedding the ring between 2 layers of collagen to avoid penetrating the 3D collagen matrix to embed the ring [39]. All these modifications helped us achieve prolific the sprouting that is essential to obtain high-quality images and reliable biochemical data.

The most common method of quantifying angiogenesis is through manual counting of the sprouts using phase contrast images [22,39]. However, this method can be inaccurate and erroneous especially if the sprout network is dense. In our improved protocol, we leverage the halo-like spread of the sprouts to draw a circumferential outline around sprouting edge to measure the radial distance of sprouting from the ring. Through further processing *via* ImageJ, this technique yields reliable, consistent and accurate means of quantifying levels of angiogenic growth from the ring center. Moreover, our second method of angiogenesis quantification allows dual measurements, one of protein levels and the other of the area of the sprout *via* fluorescence intensities of their respective labels.

Aortic ring sprouts have been generally visualized by labelling with antibodies against CD31, α-smooth muscle actin, and NG2, which mark endothelial cells and pericytes [22,39]. Moreover, the cell surface of endothelial cells can be efficiently labeled by fluorophore-conjugated lectins, such as IB4 [40,41]. However, imaging intracellular proteins is challenging due to the non-specific binding to the 3D collagen. To prevent this, we reduce the concentration of primary antibody and blocking agent (BSA) as BSA can bind tightly to collagen, and we implement continuous rocking to prevent debris from settling. These changes enabled us to obtain for the first-time high-resolution images of intracellular proteins. For extracellular molecules such as HA, we eliminated permeabilization to avoid disrupting the integrity of extracellular structures. Overall, our improved aortic ring assay provides a robust tool for characterizing angiogenesis. A summary of advantages and limitations are listed below.

*Advantages*

- High number of sprouted rings (~90% sprouted rings) is obtained which makes the assay very scalable and efficient.
- Rings are amenable to inhibitor/drug treatment and present a convenient platform to study mechanism of signaling pathways.
- Ease of obtaining sub-cellular, molecular level details in micro-vessels by acquiring high-resolution intracellular and extracellular protein images.

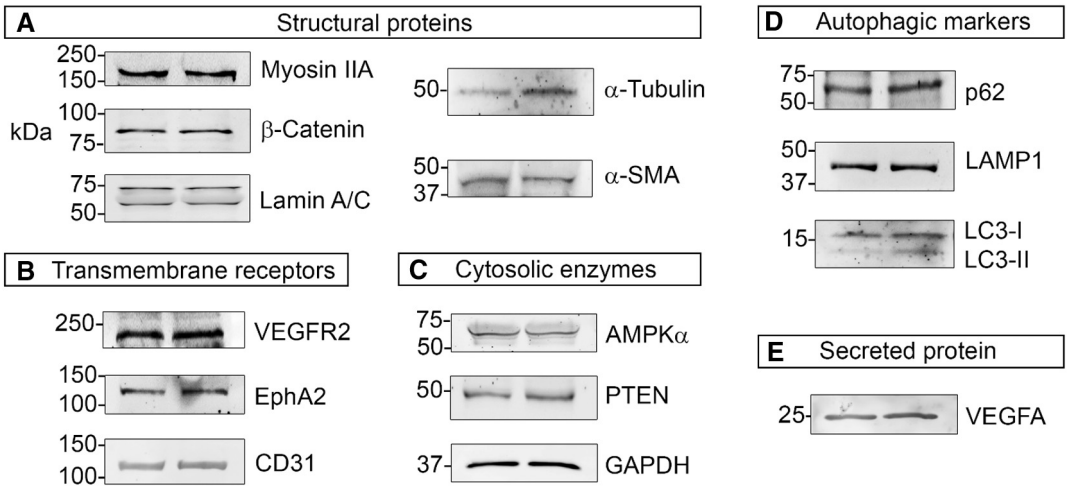


**Fig. 4.** Immunoblot detection of proteins in lysates of aortic ring sprouts. WB immunoblots of (A) structural proteins, (B) transmembrane receptors, (C) cytosolic enzymes, (D) autophagic markers and (E) secreted protein. Immunoblots includes two technical replicates extracted from aortic ring sprouts incubated until day 5–7.

- Reliable biochemical analysis of rare proteins such as phosphorylated kinases and enzymes.

*Limitations*

- Quantification method only measures the overall change in angiogenesis and does not differentiate between the length and number of sprouts.
- Vessel maturation is not achieved due to the absence of blood flow, so the data should be interpreted within the context of the assay.
- Sprouts tend to regress after eleven days of culture. Therefore, the window of treatment and analysis is limited.

## Conclusion

Our modifications to the aortic ring assay allow higher reproducibility due to improved sprouting and branching. Our staining procedure has greatly advanced our ability to see intracellular and extracellular matrix proteins with high resolution in *ex vivo* angiogenic model. We have also optimized the biochemical analysis of the ring to measure low levels of proteins such as the phosphorylated forms of signaling molecules. Hence, our modifications to the aortic ring assay have significantly advanced the knowledge of the angiogenic models.

## Materials

### Preparation of 3D collagen type I matrix and aortic ring dissection

We used rat-tail collagen type I (Millipore 08-115 or GIBCO A10483-01); media 199 10× phenol red free (ThermoFisher); 140 mM $NaHCO_3$ (filter sterilized); 1 M NaOH; filtered and autoclaved water. Forty-eight-well cell culture plates (Corning); EGM-2 MV media and supplement (Lonza CC3156 and CC4147); EnGS endothelial cell media and supplement (VascuLife LM-0002 and LS-1019); stereoscopic microscope (Fischer scientific); Hank's balanced salt solution (Corning 21-020-CM). We used C57BL/6 J mice in all our experiments.

### Aortic ring staining

We used 4% paraformaldehyde; phosphate buffered saline; bovine serum albumin (Fischer BP9705); Triton X-100 (Sigma T8787); Isolectin GS-IB4 AF594 conjugate (ThermoFisher I32450); rabbit polyclonal anti-CD31 antibody (Abcam ab28364); DAPI (Sigma 9542); rabbit monoclonal P-PERK antibody (Abcam ab192591), biotinylated-HABP (Sigma H385911); mouse monoclonal anti-HAS2 antibody (Santa Cruz sc-365263); AlexaFluor594 donkey anti-rabbit (Invitrogen A21207); AlexaFluor488 goat anti-mouse (Invitrogen A11029); Confocal/multiphoton microscope (Zeiss LSM780).

### Acquisition of vessel sprout lysates

We dissolved the 3D gels containing the sprouts in a modified RIPA buffer composed of: Tris HCl, pH 7.5 (50 mM), NaCl (150 mM), EGTA and EDTA (1 mM each), 1% Triton X-100, 0.5% Na-deoxycholate, 0.5% SDS, Na-orthovanadate (1 mM), one EDTA-free protease tablet (ThermoFisher A32965), leupeptin and aprotinin (1 μg/ml each), tosyl phenylalanyl chloromethyl ketone (TPCK, 100 μM), phenylmethylsulfonyl fluoride (PMSF,1 mM), 5× sample buffer (see Note 13). Primary antibodies include: Myosin IIA rabbit polyclonal antibody (CST 3403); β-Catenin rabbit polyclonal

antibody (Abcam ab16051); Lamin A/C rabbit polyclonal antibody (CST 2032S); α-Tubulin mouse monoclonal antibody (Santa Cruz sc-8035); α-SMA mouse monoclonal antibody (Sigma A2547); VEGFR2 (55B11) rabbit monoclonal antibody (CST 2479); EphA2 rabbit polyclonal antibody (Santa Cruz sc-924) (Santa Cruz C-20); CD31 rabbit polyclonal antibody (Abcam ab28364); AMPKα rabbit monoclonal antibody (CST 2532S); GAPDH rabbit monoclonal antibody (CST 2118S); PTEN rabbit monoclonal antibody (CST 138G6); p62 rabbit polyclonal antibody (Sigma P0068); LAMP1 rabbit monoclonal antibody (Abcam ab108597); LC3 A/B rabbit polyclonal antibody (Sigma L7543); VEGFA mouse monoclonal (Santa Cruz sc-7269). Secondary antibodies include: Goat anti-rabbit HRP-conjugated (EMD Millipore AP307P); Goat anti-mouse HRP-conjugated (EMD Millipore AP308P).

## Author contribution

All the authors conceptualized the idea, performed experiments and participated in writing the manuscript.

## Declaration of competing interest

The authors state no conflict of interest.

## Acknowledgements

We thank all the members of the Iozzo's laboratory for their constructive feedback in improving the manuscript. The original research was supported in part by NIH CA39481 and CA47282 (to RVI). Carolyn Chen was supported in part by NIH training grants T32 AR052273.

*Received 20 December 2019;*
*Received in revised form 16 January 2020;*
*Accepted 18 January 2020*
Available online 4 February 2020

***Keywords:***
Extracellular matrix;
Aortic rings;
Collagen;
Sprouts;
Endothelial cell markers;
Hyaluronan binding protein

***Abbreviations used:***
PFA, paraformaldehyde; ECM, extracellular matrix; HA, hyaluronan; HABP, HA-binding protein; IB4, *Griffonia simplicifolia* isolectin B4; PBS, phosphate buffered saline; DAPI, 4′,6-diamidine-2′-phenylindole dihydrochloride; PERK, protein kinase R-like endoplasmic reticulum kinase; RIPA buffer, radioimmunoprecipitation assay buffer.

## References

[1] J. Hutchenreuther, K. Vincent, C. Norley, M. Racanelli, S.B. Gruber, T.M. Johnson, et al., Activation of cancer-associated fibroblasts is required for tumor neovascularization in a murine model of melanoma, Matrix Biol. 74 (2018) 52–61.
[2] E. Andreuzzi, R. Colladel, R. Pellicani, G. Tarticchio, R. Cannizzaro, P. Spessotto, et al., The angiostatic molecule Multimerin 2 is processed by MMP-9 to allow sprouting angiogenesis, Matrix Biol. 64 (2017) 40–53.
[3] C.J. Turner, K. Badu-Nkansah, R.O. Hynes, Endothelium-derived fibronectin regulates neonatal vascular morphogenesis in an autocrine fashion, Angiogenesis. 20 (2017) 519–531.
[4] S. Yu, S. Yao, Y. Wen, Y. Wang, H. Wang, Q. Xu, Angiogenic microspheres promote neural regeneration and motor function recovery after spinal cord injury in rats, Sci. Rep. 6 (2016) 33428.
[5] R.V. Iozzo, I. Cohen, Altered proteoglycan gene expression and the tumor stroma, Experientia 49 (1993) 447–455.
[6] R.V. Iozzo, J.D. San Antonio, Heparan sulfate proteoglycans: heavy hitters in the angiogenesis arena, J. Clin. Invest. 108 (2001) 349–355.
[7] M.A. Gubbiotti, T. Neill, R.V. Iozzo, A current view of perlecan in physiology and pathology: a mosaic of functions, Matrix Biol. 57–58 (2017) 285–298.
[8] N.K. Karamanos, A.D. Theocharis, T. Neill, R.V. Iozzo, Matrix modeling and remodeling: a biological interplay regulating tissue homeostasis and diseases, Matrix Biol. 75–76 (2019) 1–11.
[9] N.K. Karamanos, Z. Piperigkou, A.D. Theocharis, H. Watanabe, M. Franchi, S. Baud, et al., Proteoglycan chemical diversity drives multifunctional cell regulation and therapeutics, Chem. Rev. 118 (2018) 9152–9232.
[10] L. Schaefer, Decoding fibrosis: mechanisms and translational aspects, Matrix Biol. 68–69 (2018) 1–7.
[11] S.C. MacLauchlan, N.E. Calabro, Y. Huang, M. Krishna, T. Bancroft, T. Sharma, et al., HIF-1α represses the expression of the angiogenesis inhibitor thrombospondin-2, Matrix Biol. 65 (2018) 45–58.
[12] F. Galvagni, F. Nardi, O. Spiga, A. Trezza, G. Tarticchio, R. Pellicani, et al., Dissecting the CD93-Multimerin 2 interaction involved in cell adhesion and migration of the activated endothelium, Matrix Biol. 64 (2017) 112–127.
[13] R. Lugano, K. Vemuri, D. Yu, M. Bergqvist, A. Smits, M. Essand, et al., CD93 promotes beta1 integrin activation and fibronectin fibrillogenesis during tumor angiogenesis, J. Clin. Invest. 128 (2018) 3280–3297.
[14] R.V. Iozzo, M.A. Gubbiotti, Extracellular matrix: the driving force of mammalian diseases, Matrix Biol. 71–72 (2018) 1–9.
[15] C. Chen, A. Kapoor, R.V. Iozzo, Methods for monitoring matrix-induced autophagy, Methods Mol. Biol. 1952 (2019) 157–191.
[16] M. Mongiat, S. Buraschi, E. Andreuzzi, T. Neill, R.V. Iozzo, Extracellular matrix: the gatekeeper of tumor angiogenesis, Biochem. Soc. Trans. 47 (2019) 1543–1555.
[17] R.A. Fenton, L. Brond, S. Nielsen, J. Praetorius, Cellular and subcellular distribution of the type-2 vasopressin receptor in the kidney, Am. J. Physiol Renal Physiol 293 (2007) F748–F760.

[18] A.D. Theocharis, N.K. Karamanos, Proteoglycans remodeling in cancer: underlying molecular mechanisms, Matrix Biol. 75–76 (2019) 220–259.
[19] L. Schaefer, C. Tredup, M.A. Gubbiotti, R.V. Iozzo, Proteoglycan neofunctions: regulation of inflammation and autophagy in cancer biology, FEBS J. 284 (2017) 10–26.
[20] R.F. Nicosia, R. Tchao, J. Leighton, Histotypic angiogenesis in vitro: light microscopic, ultrastructural, and radioautographic studies, In Vitro 18 (1982) 538–549.
[21] R.F. Nicosia, J.A. Madri, The microvascular extracellular matrix. Developmental changes during angiogenesis in the aortic ring-plasma clot model, Am. J. Pathol. 128 (1987) 78–90.
[22] R.F. Nicosia, The aortic ring model of angiogenesis: a quarter century of search and discovery, J. Cell. Mol. Med. 13 (2009) 4113–4136.
[23] S. Blacher, L. Devy, M.F. Burbridge, G. Roland, G. Tucker, A. Noel, et al., Improved quantification of angiogenesis in the rat aortic ring assay, Angiogenesis. 4 (2001) 133–142.
[24] G. Alessandri, M. Girelli, G. Taccagni, A. Colombo, R. Nicosia, A. Caruso, et al., Human vasculogenesis ex vivo: embryonal aorta as a tool for isolation of endothelial cell progenitors, Lab. Investig. 81 (2001) 875–885.
[25] V.E. Van, R.H. De, L. Devy, S. Blacher, C. Munaut, A. Noel, et al., Murine 5T multiple myeloma cells induce angiogenesis in vitro and in vivo, Br. J. Cancer 86 (2002) 796–802.
[26] Z. Shao, M. Friedlander, C.G. Hurst, Z. Cui, D.T. Pei, L.P. Evans, et al., Choroid sprouting assay: an ex vivo model of microvascular angiogenesis, PLoS One 8 (2013) e69552.
[27] O. Gealekman, A. Burkart, M. Chouinard, S.M. Nicoloro, J. Straubhaar, S. Corvera, Enhanced angiogenesis in obesity and in response to PPARgamma activators through adipocyte VEGF and ANGPTL4 production, Am. J. Physiol. Endocrinol. Metab. 295 (2008) E1056–E1064.
[28] S. Goldoni, D.G. Seidler, J. Heath, M. Fassan, R. Baffa, M.L. Thakur, et al., An anti-metastatic role for decorin in breast cancer, Am. J. Pathol. 173 (2008) 844–855.
[29] S.J. Gauci, S.B. Golub, L. Tatarczuch, E. Lee, D. Chan, N.C. Walsh, et al., Disrupted type II collagenolysis impairs angiogenesis, delays endochondral ossification and initiates aberrant ossification in mouse limbs, Matrix Biol. 83 (2019) 77–96.
[30] J. Koivunen, A.V. Kemppainen, M.A. Finnila, R. Keski-Filppula, H. Haronen, H. Tu, et al., Collagen XIII-derived ectodomain regulates bone angiogenesis and intracortical remodeling, Matrix Biol. 83 (2019) 6–25.
[31] S.C. MacLauchlan, N.E. Calabro, Y. Huang, M. Krishna, T. Bancroft, T. Sharma, et al., HIF-1alpha represses the expression of the angiogenesis inhibitor thrombospondin-2, Matrix Biol. 65 (2018) 45–58.
[32] O. Burgy, M. Konigshoff, The WNT signaling pathways in wound healing and fibrosis, Matrix Biol. 68–69 (2018) 67–80.
[33] A.A. Dunkman, M.R. Buckley, M.J. Mienaltowski, S.M. Adams, S.J. Thomas, L. Satchell, et al., Decorin expression is important for age-related changes in tendon structure and mechanical properties, Matrix Biol. 32 (2013) 3–13.
[34] S. Patel, M. Santra, D.J. McQuillan, R.V. Iozzo, A.P. Thomas, Decorin activates the epidermal growth factor receptor and elevates cytosolic $Ca^{2+}$ in A431 cells, J. Biol. Chem. 273 (1998) 3121–3124.
[35] S. D'hondt, B. Guillemyn, D. Syx, S. Symoens, R.R. De, L. Vanhoutte, et al., Type III collagen affects dermal and vascular collagen fibrillogenesis and tissue integrity in a mutant Col3a1 transgenic mouse model, Matrix Biol. 70 (2018) 72–83.
[36] E. Brauchle, J. Kasper, R. Daum, N. Schierbaum, C. Falch, A. Kirschniak, et al., Biomechanical and biomolecular characterization of extracellular matrix structures in human colon carcinomas, Matrix Biol. 68-69 (2018) 180–193.
[37] G. Chiaverina, B.L. di, V. Monica, M. Accardo, M. Palmiero, B. Peracino, et al., Dynamic interplay between pericytes and endothelial cells during sprouting angiogenesis, Cells 8 (2019).
[38] A.C. Aplin, R.F. Nicosia, The plaque-aortic ring assay: a new method to study human atherosclerosis-induced angiogenesis, Angiogenesis. 22 (2019) 421–431.
[39] M. Baker, S.D. Robinson, T. Lechertier, P.R. Barber, B. Tavora, G. D'Amico, et al., Use of the mouse aortic ring assay to study angiogenesis, Nat. Protoc. 7 (2012) 89–104.
[40] C. Ernst, B.R. Christie, Isolectin-IB 4 as a vascular stain for the study of adult neurogenesis, J. Neurosci. Methods 150 (2006) 138–142.
[41] R.L. Benton, M.A. Maddie, D.R. Minnillo, T. Hagg, S.R. Whittemore, Griffonia simplicifolia isolectin B4 identifies a specific subpopulation of angiogenic blood vessels following contusive spinal cord injury in the adult mouse, J. Comp. Neurol. 507 (2008) 1031–1052.